

How tissue optics affect dosimetry of photodynamic therapy

Steven L. Jacques

Oregon Health and Science University
Departments of Dermatology and Biomedical
Engineering
Portland, Oregon 97239-4501

Abstract. We describe three lessons learned about how tissue optics affect the dosimetry of red to near-infrared treatment light during PDT, based on working with Dr. Tayyaba Hasan. Lesson 1—The optical fluence rate ϕ near the tissue surface exceeds the delivered irradiance (E). A broad beam penetrates into tissue to a depth (z) as $\phi = Eke^{-\mu z}$, with an attenuation constant μ and a backscatter term k . In tissues, k is typically in the range 3–5, and $1/\mu$ equals δ , the $1/e$ optical penetration depth. Lesson 2—Edge losses at the periphery of a uniform treatment beam extend about 3δ from the beam edge. If the beam diameter exceeds 6δ , then there is a central zone of uniform fluence rate in the tissue. Lesson 3—The depth of treatment is linearly proportional to δ (and the melanin content of pigmented epidermis in skin) while proportional to the logarithm of all other factors, such as irradiance, exposure time, or the photosensitizer properties (concentration, extinction coefficient, quantum yield for oxidizing species). The lessons illustrate how tissue optics play a dominant role in specifying the treatment zone during PDT. © 2010 Society of Photo-Optical Instrumentation Engineers. [DOI: 10.1117/1.3494561]

Keywords: photodynamic therapy; dosimetry; tissue optics; optical properties.

Paper 10009SSR received Jan. 8, 2010; revised manuscript received Jul. 10, 2010; accepted for publication Aug. 17, 2010; published online Oct. 12, 2010.

1 Introduction

This paper is a contribution to the special issue honoring Tayyaba Hasan for her significant contributions to photodynamic therapy (PDT). In the mid-1980s and early 1990s, the author had the opportunity to work with Tayyaba Hasan on the dosimetry of PDT. Those were interesting times when the dosimetry of light in tissues was first developed. Concepts of light transport now considered obvious were not so obvious then. During 1994 to 2000, the author would step into Tayyaba's annual short course on PDT held at the SPIE Photonics West Meeting to watch her teach the class and to give a short summary of the optical dosimetry of PDT. This paper summarizes three key lessons learned during during those short courses.¹

2 Lesson 1: Broad-Beam Treatment

Often a broad uniform beam of treatment light is delivered to a tissue site for the purpose of PDT. A simple description of 1-D light penetration into the tissue is appropriate,²

$$\phi(z) = Eke^{-\mu z}, \quad (1)$$

where $\phi(z)$ (in watts per centimeters squared) is the fluence rate as a function of depth z (in centimeters), E (in watts per centimeters squared) is the delivered irradiance, k is a backscatter term that describes how backscattered light augments

the E delivered to the surface to yield an elevated fluence rate near the surface, and μ [cm^{-1}] is an apparent attenuation coefficient. When the reflectance of light by the tissue exceeds ~ 0.20 , the value of μ becomes equal to $\mu_{\text{eff}} = \sqrt{3\mu_a(\mu_a + \mu'_s)}$, where μ_a is the absorption coefficient and $\mu'_s = \mu_s(1-g)$ is the reduced scattering coefficient, in which μ_s is the scattering coefficient and g is the anisotropy of scattering. As reflectance drops below 0.2 toward 0, μ approaches μ_a . For a red to near-infrared treatment light, reflectance usually exceeds 0.20.

Figure 1 illustrates the light distribution in a generic tissue generated by Monte Carlo simulations.³ The curves of relative fluence rate, $\phi(z)/E$, were generated by varying the absorption coefficient (circles: $\mu_a = 0.001\text{--}8 \text{ cm}^{-1}$, refractive index ratio $n_{\text{tissue}}/n_{\text{air}} = 1.37$) while holding the scattering properties constant ($\mu_s = 100 \text{ cm}^{-1}$, $g = 0.90$). The dashed lines are the fits to the simulated data using Eq. (1). The simulated data near the tissue surface deviate from Eq. (1), but deeper in the tissue Eq. (1) provides an accurate description of the penetrating treatment light. Not shown, but later used in Fig. 2, are similar curves where μ_s was reduced from 100 to 10 cm^{-1} or 1 cm^{-1} , so that the ratio μ'_s/μ_a would drop and the reflectance would approach zero.

Figure 2 shows the behavior of k and μ in Eq. (1), as applied to the data in Fig. 1. Figure 2(a) plots the values of k versus the total diffuse reflectance (R_d). In the limit of $R_d = 0$, the value of k is 1. As R_d increases, the backscatter toward the surface increases, indicated by the steady rise in k .

Address all correspondence to: Steven L. Jacques, Oregon Health and Science University, 3303 SW Bond Avenue, Portland, Oregon 97239; Tel: 503-418-9338; E-mail: jacquess@ohsu.edu

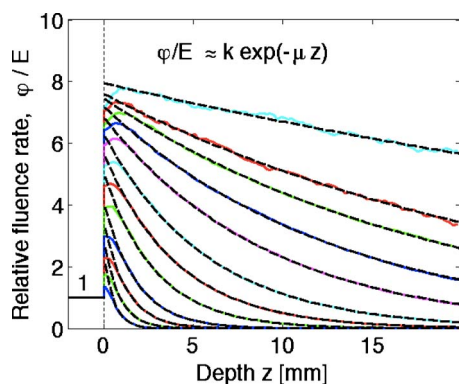


Fig. 1 One-dimensional relative fluence rate, $\phi(z)/E$, where E (in watts per centimeters squared) is the irradiance delivered as a broad uniform beam. The dashed lines correspond to Eq. (1). The colored lines are Monte Carlo simulations, using the optical properties $\mu_s = 100 \text{ cm}^{-1}$ and $g=0.90$, such that $\mu_s(1-g)=10 \text{ cm}^{-1}$, and μ_a varies from 0.01 to 8 cm^{-1} .

The maximum value of k is ~ 8.4 when R_d approaches 1.0. To reach the limit of $R_d \approx 1$, μ_a must approach 0 while μ'_s has a finite value. In this limit, all the light must eventually be reflected from the tissue although complete escape may take a long time. The photons still spend time in the tissue before escaping. Hence, the rate at which the light passes through the air/tissue interface at the tissue surface to escape as observable R_d is also finite. In other words, fluence rate near the surface is finite. The Monte Carlo simulations indicate this limiting value for k is ~ 8.4 , a value that depends on the refractive index mismatch at the tissue surface.

Figure 2(b) plots the values of $\phi(0)/E$ at the surface ($z=0$) versus R_d . The relation is linear. When R_d is zero, $\phi(0)/E=1$. In other words, there is no augmentation of near-surface fluence rate by backscatter. As R_d increases, the backscatter increases $\phi(0)$. Because the reflectance of red PDT treatment light by tissues is typically in the range 0.2–0.6, the value of $\phi(0)$ can be 2.4-fold to 5.1-fold greater than the delivered irradiance E .

Figure 2(c) plots the values of μ/μ_{eff} versus R_d . Above $R_d \approx 0.20$, μ/μ_{eff} equals unity; hence, $\mu = \mu_{\text{eff}}$. In the limit of very low R_d , the value of μ approaches μ_a , and the value of μ_{eff} is $\mu_a \sqrt{3}$. Therefore, μ/μ_{eff} approaches $1/\sqrt{3}$ as R_d approaches zero. For PDT treatment with red to near-infrared light, R_d exceeds 0.20 so μ equals μ_{eff} or $1/\delta$, where δ is the $1/e$ optical penetration depth.

A measurement of R_d can characterize the parameters k and $\phi(0)$ that specify the light dosimetry. The total diffuse reflectance R_d can be approximated by the simple expression,

$$R_d \approx e^{-\mu_a \delta} = e^{-8/\sqrt{3[1+(\mu'_s/\mu_a)]}}. \quad (2)$$

This expression has the form of a simple exponential attenuation of photons that travel a pathlength 8δ within a tissue with absorption coefficient μ_a . Although the factor 8 is only an approximate value, Eq. (2) yields R_d with a $<5\%$ error for red to near-infrared wavelengths used for PDT. The factor 8 varies with the ratio μ'_s/μ_a , as has been described.⁴

The key lesson is that the fluence rate within the tissue near the surface, $\phi(0)$, significantly exceeds the delivered ir-

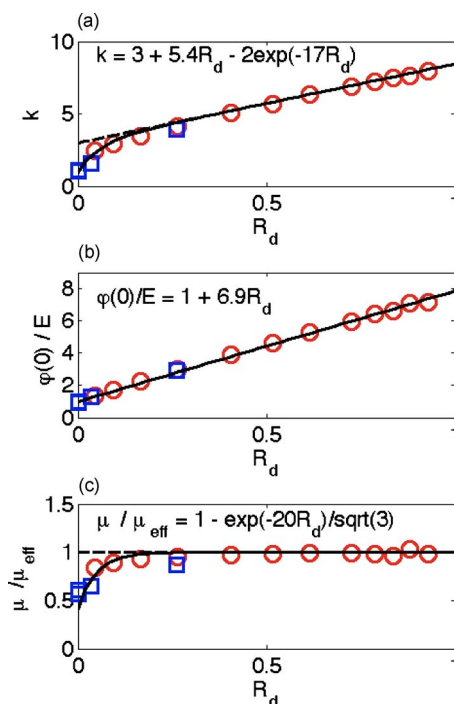


Fig. 2 (a) Backscatter parameter k versus diffuse reflectance R_d . (b) The relative fluence rate, $\phi(0)/E$, at the tissue surface, where E is the delivered irradiance, versus R_d . (c) The ratio of attenuation coefficient (μ) to effective attenuation coefficient (μ_{eff}) versus R_d . Circles are for $\mu'_s = 10 \text{ cm}^{-1}$, with varying μ_a values, as in Fig. 1. Squares are for $\mu'_s = 1 \text{ cm}^{-1}$, not shown in Fig. 1. Lines are curve fits by equations shown in figures.

radiance, E . The light accumulates near the surface due to backscatter, which augments the fluence rate at the surface by the factor k in Eq. (1). This augmentation factor k increases as R_d increases, becoming linearly proportional to R_d when reflectance exceeds 0.20, as is the case for PDT treatment with red to near-infrared light. The penetration of fluence rate into the tissue follows the simple exponential of Eq. (1), as if an irradiance kE had been delivered to the surface. The actual fluence rate at the surface, $\phi(0)$, is lower than kE . The deeply penetrating light for $z > \delta$ accurately follows Eq. (1).

Today, this accumulation of light at a tissue surface seems rather obvious. But back in the 1980s, the idea that backscatter would augment delivered light such that the factor k in Eq. (1) was >1 was not widely appreciated. Indeed, Star and I presented an experimental demonstration at a Gordon conference on lasers in medicine and biology in the 1980s in which we placed an isotropic probe⁵ (see Fig. 3) within a beaker of milk near the front surface that was irradiated with light. We demonstrated to the audience that the fluence rate ϕ in the front surface layer of milk was threefold higher than the delivered irradiance E , which surprised many in the audience. Figure 4 shows an experiment that recreated this demonstration.

In a similar experiment with a live mouse, conducted with Hasan, the isotropic probe was placed below the skin in the peritoneal cavity of a white mouse and a broad beam of 630 nm light delivered. The ϕ was measured and the ratio ϕ/E was 1.4 ± 0.4 (mean \pm standard deviation for ~ 10

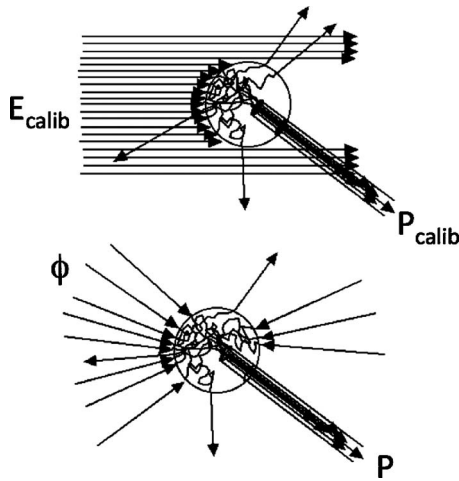


Fig. 3 Optical fiber inserted in a turbid plastic ball ($\sim 0.9\text{-}\mu\text{m}$ -diam) collected light with equal efficiency from all angles. Calibration of the probe involved inserting the probe into a cuvette of water, irradiating with a known irradiance E_{calib} , and measuring P_{calib} . Then insertion in turbid medium or tissue yielded a measurement P that specified the fluence rate: $\phi = PE_{\text{calib}}/P_{\text{calib}}$. (Drawing of the probe fabricated by H. Marijnissen and W. Star, Daniel Den Hoed Cancer Center, Rotterdam, who provided the probe for experiments.)

measurements); in other words, there was more light below the skin than was delivered to the surface. This is not a violation of conservation of energy, but simply an accumulation of delivered light near the surface layers of a tissue.

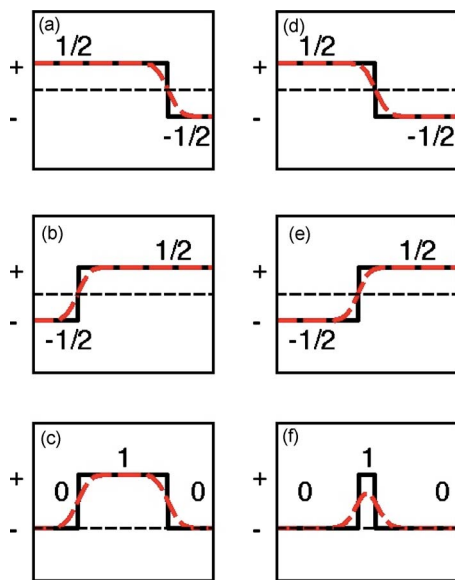


Fig. 4 A fish tank was filled with clear water, and a broad collimated laser irradiated the front surface. An isotropic probe (Fig. 3) measured the fluence rate axially as the probe was moved by a screw assembly from the front to the rear of the tank. The fluence rate within the tank was uniform at value 1 (curve A). Then, milk and ink were added, and the scattering caused light to pile up near the front surface (curve B). When water replaced air in the front compartment, D, the total internal reflectance at the front surface was reduced, and the fluence rate slightly dropped (curved C). (Experiment conducted with Marleen Keijzer, Delft University, The Netherlands.)

A final word on the limitations of Eqs. (1) and (2) is needed. The expressions for the 1-D penetration of light into tissue [Eq. (1)] and the reflectance of light [Eq. (2)] are based on Monte Carlo simulations, which properly handle the computation of fluence rate near the air/tissue surface boundary. The results reported here are for the case of $n_{\text{tissue}} = 1.4$. If the n_{tissue} varies, then the dosimetry will also change slightly. If n_{tissue} decreases, which would occur if a tissue were edematous, then the ratio $n_{\text{tissue}}/n_{\text{air}}$ would drop slightly and light would escape more easily from the tissue. Therefore, k and $\phi(0)$ would slightly drop in Eq. (1). Another issue is how a rough tissue surface will affect total internal reflectance at the air/tissue surface.⁶ A rough surface decreases total internal reflectance, which again would cause k and $\phi(0)$ to slightly drop. Another caveat is needed when the total diffuse reflectance R_d drops below 0.25, which indicates the ratio μ'_s/μ_a has dropped below 10. At such low reflectance, the influence of the anisotropy of scattering (g) becomes more important, and the simple expression of Eq. (2) becomes slightly dependent on the value of g . The results reported here are for $g = 0.90$, which is appropriate for most tissues in the red to near-infrared spectrum. As g drops to lower values, the value 8 in Eq. (2) drops. All these effects are minor and do not alter the usefulness of Eq. (2) or the lessons of this first section. In summary, Eqs. (1) and (2) instruct regarding the general behavior of light dosimetry, but slight variations may occur.

3 Lesson 2: Beam Edge Effects

The depth of penetration also depends on the diameter of the treatment beam. Delivered light spreads within a tissue, both along the radial direction r and the depth direction z . In the middle of a very broad beam of delivered light, the lateral diffusion of light from neighboring points of light injection is balanced and cancels; thus, there is no lateral variation in fluence rate. Only variation versus depth occurs, as discussed above. With a finite-diameter beam, the edge of the beam has no neighbors outside the beam, and lateral diffusion is unbalanced, and there are edge losses.

The process is illustrated schematically in Fig. 5. A finite-diameter uniform-irradiance beam (full width= w) is treated as the sum of two sources (black solid lines), where one source has positive uniform irradiance over a semi-infinite range in one direction, $E = +1/2$ for $x < -w/2$, and a negative uniform irradiance in the other direction, $E = -1/2$ for $x > -w/2$. The second source has the opposite configuration, negative to the left, $E_2 = -1/2$ for $x < +w/2$, and positive to the right, $E_2 = +1/2$ for $x > +w/2$. This model is a mathematical construct because there is no physical realization of a negative irradiance. The red dashed lines show the fluence rate (ϕ) in the tissue, which is subject to the lateral diffusion of light at the edges of the two sources. This ϕ can be the $\phi(0)$ at the surface where ϕ exceeds E , or some $\phi(z)$ within the tissue. Both the E and ϕ are normalized so they can be drawn as extending between $\pm 1/2$. Again, this is a mathematical construct. The fluence rate ϕ is modeled as an error function: $\phi_1 = 0.5\{\text{erfc}[(x-w/2)/\delta] - 1\}/2$, and $\phi_2 = 0.5\{\text{erfc}[(x+w/2)/\delta] + 1\}/2$, where δ is the $1/e$ attenuation length equal to $1/\mu_{\text{eff}}$. The factor x is a lateral position on the tissue. The total beam is the sum of the two sources, E_{total}

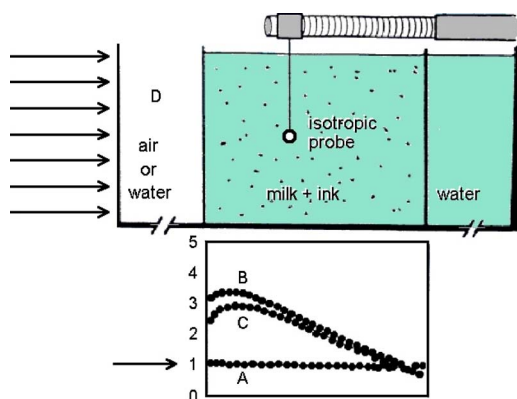


Fig. 5 Overlap of losses at the edges of a finite-diameter uniform-irradiance beam. Schematic illustration of how a finite-diameter treatment beam of uniform irradiance can be modeled as the superposition of two semi-infinite beams that vary between $+E/2$ and $-E/2$, where E is the irradiance. This is a mathematical construct, because there is no physical occurrence of a negative irradiance. One beam (A,D) extends positively to the left. The second beam (B,E) extends positively to the right. The irradiance E is portrayed as a solid black line, normalized by its maximum value, $0.5E/\max(E)$, so that the black line varies from $+1/2$ to $-1/2$. The resulting fluence rate ϕ is shown as a dashed red line. This ϕ could be $\phi(0)$ at the surface, which exceeds E , or ϕ could be $\phi(z)$ at some depth z . In this figure, ϕ is normalized by its maximum value, $0.5\phi/\max(\phi)$, so that it also varies from $+1/2$ to $-1/2$. Again, there is no physical negative fluence rate. The sum of the two beams, $C=A+B$, and $F=D+E$, yields the fluence rate ϕ that results from a finite-diameter beam. The ϕ achieves a maximum value, $\phi/\max(\phi)=1$, in the central region when the beam is broad, and a value of 0 far outside the beam. When the beam diameter is narrow, the edge effects overlap and superimpose, which diminishes the fluence rate of the central region. (Color online only.)

$=E_1+E_2$, which equals 1 within the beam and 0 outside the beam. The total fluence rate for the total beam is $\phi_{\text{total}}=\phi_1+\phi_2$. For a broad beam ($w/2\gg 3\delta$), the central region of the beam achieves the maximum ϕ . The edge losses are far apart and do not interact, leaving a central region of maximum fluence rate. For the narrow beam, the edge losses overlap and combine to limit the fluence rate in the central region.

Figure 6 shows Monte Carlo simulations of the depth and lateral spread of light in a generic tissue. The beam is uniform and its radius is increased from 0 to 1–2 cm. The total beam power is kept constant at 1 W. The isofluence contours for a range of fluence rates are shown. The deepest penetration occurs with the narrowest beam because all the light is concentrated in one spot, but the light distribution is not uniform. As the beam broadens, the penetration of light decreases because the light is being spread out over the tissue. However, a central region of uniform fluence rate and penetration develops in the center of the beam, when the beam radius exceeds 3δ .

The lesson learned is that tissue optics specify the optimal size of the treatment beam to achieve a central region of uniform fluence rate within the tissue, where Eq. (1) applies. A treatment beam diameter should exceed the diameter of the target tissue by 6δ to ensure a central region of uniform light exposure at the target. The total power of the treatment light can be increased to achieve the desired fluence rate at the target depth.

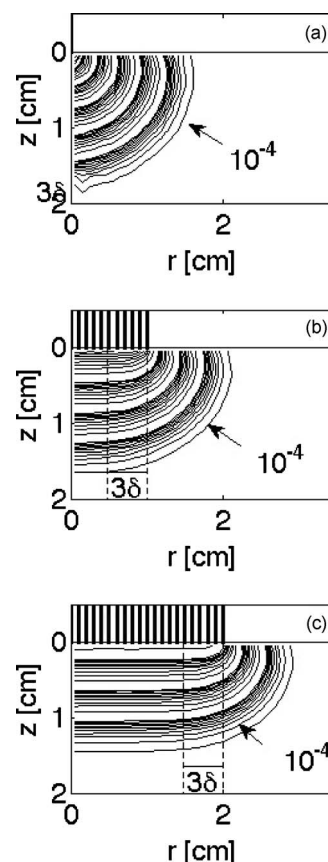


Fig. 6 Monte Carlo simulation of fluence rate [ϕ (in watts per centimeters squared)] within a generic tissue, showing iso- ϕ contours versus depth z and radial position r , starting at 10^{-4} W/cm², and increasing over four orders of magnitude. A 1-W treatment beam is delivered as (a) a narrow beam, (b) a 1-cm-radius beam, or (c) a 2-cm-radius beam. The vertical dashed lines show the edge of the beam and the position $r=\text{radius}-3\delta$, within which a central region of uniform ϕ occurs ($\mu_a=1$ cm⁻¹, $\mu_s=100$ cm⁻¹, $g=0.90$, $n_{\text{tissue}}=1.4$, $\delta=0.174$ cm, $3\delta=0.552$ cm).

4 Lesson 3: PDT Dosimetry

The light dose that generates photodynamic action is described by the fluence, H (in joules per centimeters squared), which equals the fluence rate ϕ (in watts per centimeters squared) times the exposure time t (in seconds): $H=\phi t$. Although tissue damage by oxidation (via necrosis or apoptosis) is a stochastic event governed by the fluence, in experiments one often sees a boundary of damage, which suggests the practical concept of a threshold fluence (H_{th}) that causes damage. Therefore, it is useful to assume a threshold radiant exposure H_{th} , such that if H exceeds H_{th} then the PDT treatment achieves cell death either through necrosis or apoptosis, or achieves the particular endpoint of interest (see Fig. 7).

Similar to Eq. (1) the fluence rate $H(z)$ drops with depth and reaches H_{th} at a depth z_{Rx} that corresponds to the margin of treatment (the subscript Rx indicates effective treatment),

$$H_{\text{th}} = Etke^{-z_{\text{Rx}}/\delta}. \quad (3)$$

Rearranging Eq. (3) to solve for z_{Rx} ,

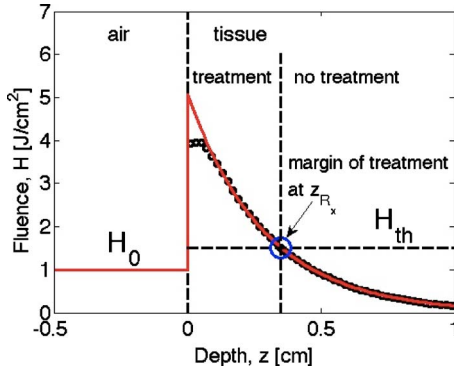


Fig. 7 Dosimetry of PDT specifies the depth of treatment, z_{Rx} , based on Eq. (3) that relates the delivered radiant exposure H_0 (in joules per centimeters squared) and the light penetration (depends on k and μ) versus the threshold fluence H_{th} that elicits treatment. Black circles are a Monte Carlo simulation of the fluence $H(z)$ within the tissue. The red line is the delivered H_0 and the $H(z_{Rx})$ within the tissue [see Eq. (1)]. The horizontal dashed line is the threshold H_{th} . The vertical dashed line is the boundary of the depth of treatment z_{Rx} . (Color online only.)

$$z_{Rx} = \delta \ln \left(\frac{Et k}{H_{th}} \right). \quad (4)$$

Equation (4) shows that z_{Rx} is proportional to the optical penetration depth δ , but the other factors ($Et k / H_{th}$) are compressed by the logarithm function so their influence on z_{Rx} is diminished. Doubling δ will double z_{Rx} [actually, a little better than a twofold increase since k will increase as δ increases so the factor $\ln(k)$ comes into play]. Doubling the exposure time t will only increase z_{Rx} by the increment $\delta \ln(2)$ or 0.69δ . For example, assume PDT was administered at 630 nm wavelength using an irradiance H_0 that exactly matches the lethal threshold H_{th} , which perhaps had been observed in cell culture studies where optical scattering is not an issue. Because k in Eq. (2) exceeds 1, the light near the tissue surface will exceed H_{th} . Also assume some standard optical properties for the tissue: blood volume fraction=0.013, oxygen saturation=0.75, water content=0.65, absorption coefficient $\mu_a=0.123 \text{ cm}^{-1}$, reduced scattering coefficient $\mu'_s=(20 \text{ cm}^{-1})(\lambda/630 \text{ nm})^{-1}$. Then, Eq. (4) will yield Fig. 8 showing z_{Rx} versus wavelength, using the expression for k in Fig. 2(a) that uses R_d based on Eq. (2). The z_{Rx} for the 630-nm-wavelength treatment light is 7.0 mm. If one increases the exposure time fourfold, the Eq. (4) indicates that the treatment zone will increase to 12.1 mm, a 1.72-fold greater zone of treatment. Now, increase the wavelength to 690 nm to decrease the absorption by blood. The scattering only slightly decreases, while the δ increases 1.67-fold. Again deliver $H_0=H_{th}$, using a different photosensitizer, but use the original exposure time. The new value of z_{Rx} is also 12.1 mm, the same as increasing the 630-nm treatment time by fourfold. Increasing the optical penetration 1.67-fold was equivalent to increasing the exposure time fourfold.

Equation (3) can be expanded to specifically mention the factors that determine H_{th} and affect dosimetry of PDT. A description of the threshold concentration of oxidizing species produced by PDT that elicits treatment, P_{th} (M), includes the

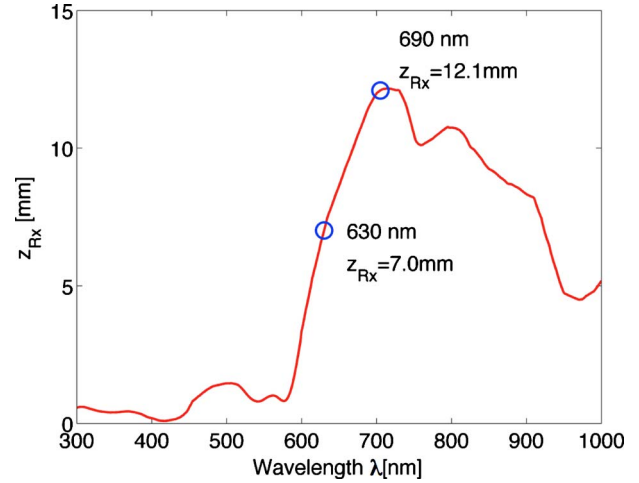


Fig. 8 Depth of treatment, z_{Rx} (in millimeters), as a function of wavelength. Approximate values using Eqs. (4) and (2) and the expression for k in Fig. 2(a) (optical properties and treatment parameters cited in text). A treatment using a 630-nm wavelength still sees significant blood absorption. Moving to a 660-nm wavelength avoids strong blood absorption and increases z_{Rx} for 7.0–12.1 mm.

extinction coefficient ϵ ($\text{cm}^{-1}\text{M}^{-1}$) for the photosensitizer, the concentration C (M) of photosensitizer, the quantum efficiency of converting excited state photosensitizer to oxidizing species (Φ , which is a function of the available oxygen), and the fraction of oxidizing species that attacks sites contributing to lethality (f_{kill}),

$$P_{th} = Et k \epsilon C \Phi f_{kill} \frac{1000\lambda}{N_A h c_0} k e^{-\mu z_{Rx}}. \quad (5)$$

The factors 1000 (in cubic centimeters per liter), wavelength λ (in centimeter), Planck's constant h (Js), and vacuum speed of light c_0 (in centimeters per second) participate in yielding units of moles per liter (M) for P_{th} . Rearranging Eq. (5) to solve for z_{Rx} and substituting the optical penetration depth δ for $1/\mu$ yields,

$$z_{Rx} = \delta \ln \left(Et k \frac{1000\lambda \epsilon C \Phi f_{kill} P_{th}}{N_A h c_0} \right). \quad (6)$$

All the factors commonly considered in clinical application of PDT, such as the irradiance, exposure time, concentration, and extinction coefficient of photosensitizer, are included within the argument of the logarithm function. The factors that specify H_{th} are clearly seen in Eq. (6).

The expression for optical penetration depth δ is

$$\delta = \frac{1}{\sqrt{3\mu_a(\mu_a + \mu'_s)}} \approx \frac{1}{\sqrt{3\mu_a\mu'_s}}, \quad (7)$$

indicating that δ is proportional to the geometric mean of μ_a and μ'_s when $\mu'_s \gg \mu_a$, which is usually the case for red to near-infrared light. A key biological factor in determining μ_a is the blood perfusion, which can easily change by a factor of 2–4. Thus, the z_{Rx} is strongly influenced by the degree of inflammation in a target tissue. A fourfold increase in blood perfusion would cause a fourfold increase in μ_a , which would

yield more than a twofold decrease in δ and hence at least a halving of the depth of treatment.

The key lesson from Eq. (6) is that the optical properties have a dominant effect on the PDT treatment zone. Equation (7) advises that changes in blood perfusion can strongly limit the treatment zone. The effort to find longer wavelength photosensitizers that absorb above 650 nm has been driven by the desire to avoid blood absorption and increase the treatment zone.

A cautionary note should be made about skin, where there may be a significantly pigmented epidermis. The melanin in the epidermis is a superficial absorber that can strongly affect the penetration of treatment light into pigmented skin. Epidermal melanin acts as a surface filter, not a volumetric absorber. Therefore, melanin presents a term $T_{\text{epi.in}} = e^{-f_{\text{v.mel}}\mu_{\text{a.mel}}L_{\text{epi.in}}}$, where $f_{\text{v.mel}}$ is the volume fraction of melanosomes in the epidermis, $\mu_{\text{a.mel}}$ is the absorption coefficient of the interior of a melanosome, and $L_{\text{epi.in}}$ is the pathlength spent by photons in the epidermis that transmit to the underlying tissue (including photons that backscatter from the dermis, totally internally reflect at the air/skin surface, and re-enter the dermis). In other words, the apparent delivered radiant exposure is $T_{\text{epi.in}}Etk$. The fluence versus depth becomes

$$H(z) = T_{\text{epi.in}}Etk e^{-\mu z} = Etk e^{-\mu z - f_{\text{v.mel}}\mu_{\text{a.mel}}L_{\text{epi.in}}} \quad (8)$$

and for $H(z_{\text{Rx}}) = H_{\text{th}}$, Eq. (8) becomes

$$z_{\text{Rx}} = \delta \left[\ln \left(\frac{Etk \epsilon C \Phi f_{\text{kill}} P_{\text{th}} 1000 \lambda}{N_A h c_0} \right) - f_{\text{v.mel}} \mu_{\text{a.mel}} L_{\text{epi.in}} \right], \quad (9)$$

which indicates that melanin content $f_{\text{v.mel}}$ also linearly affects the treatment depth z_{Rx} ($\partial z_{\text{Rx}} / \partial f_{\text{v.mel}} = -\delta f_{\text{v.mel}} \mu_{\text{a.mel}} L_{\text{epi.in}}$).

5 Discussion

What aspects of these three lessons learned still hold in current research? Lesson 1 instructs that the fluence rate within a tissue significantly exceeds the delivered irradiance, usually by a factor of 2.4- to 5.1-fold. When comparing PDT effects in cells versus tissues, one must remember that the cells receive the irradiance E while the superficial layers of a tissue receive $\phi(0) > E$. Lesson 2 instructs about the minimal width or diameter of a treatment beam to attain maximum depth of treatment, which is still pertinent to any clinical protocol involving broad beam illumination. However, the concept also extends to interstitial treatments using implanted optical fibers, whether point sources or cylindrical sources. The diffusion of light from the source again depends on δ . Investigators are developing protocols for interstitial placement of multiple

optical fibers within a solid organ, such as the prostate,^{8,9} for PDT treatments. The optical fibers that deliver light are placed in an optimal 3-D pattern to attain full coverage of the prostate volume. This work is an example of using lesson 2. Lesson 3 instructs as to the relative roles of tissue optics and the other treatment parameters involved in PDT dosimetry. The parsing of these relative roles of optics versus photosensitizer properties is inherent in the development of the concept of a PDT dose,¹⁰ which cites the number of photons absorbed by photosensitizer per gram of tissue. This dose characterizes the efficiency of a particular photosensitizer in a particular tissue.

The three lessons summarized in this paper were developed by several investigative teams around the world during the early years of PDT. This author learned the lessons while addressing issues of optical dosimetry for PDT during work with Tayyaba Hasan. She has had a great influence on many young investigators, and this author was one of those who enjoyed her collaboration. The lessons remain pertinent to current implementations of PDT and illustrate the major role that tissue optics play in determining the treatment zone.

Acknowledgment

This work was supported by NIH Grants No. R29-HL45045 and No. R01-HL084013.

References

1. T. Hasan, *Fundamentals of Photochemistry and Photodynamic Therapy*, SPIE Short Course Notes, Photonics West Symposium (1994–2000).
2. S. L. Jacques, "Simple optical theory for light dosimetry during PDT," *Proc. SPIE* **1645**, 155–165 (1992).
3. L.-H. Wang, S. L. Jacques, and L.-Q. Zheng, "MCML—Monte Carlo modeling of photon transport in multi-layered tissues," *Comput. Methods Programs Biomed.* **47**, 131–146 (1995).
4. S. L. Jacques, Diffuse reflectance from a semi-infinite medium, <http://omlc.ogi.edu/news/may99/rd/index.html> (1999).
5. J. P. A. Marijnissen and W. M. Star, "Quantitative light dosimetry *in vitro* and *in vivo*," *Lasers Med. Sci.* **2**, 235–242 (1987).
6. X. Ma, J. Q. Lu, and X.-H. Hu, "Effect of surface roughness on determination of bulk tissue optical parameters," *Opt. Lett.* **28**(22), 2204–2206 (2003).
7. S. L. Jacques and D. J. McAuliffe, "The melanosome: threshold temperature for explosive vaporization and internal absorption coefficient during pulsed laser irradiation," *Photochem. Photobiol.* **53**, 769–776 (1991).
8. A. Johansson, J. Axelsson, S. Andersson-Engels, and J. Swartling, "Realtime light dosimetry software tools for interstitial photodynamic therapy of the human prostate," *Med. Phys.* **34**(11), 4309–4321 (2007).
9. S. R. Davidson, R. A. Weersink, M. A. Haider, M. R. Gertner, A. Bogaards, D. Giewercer, A. Scherz, M. D. Sherar, M. Elhilali, J. L. Chin, J. Trachtenberg, and B. C. Wilson, "Treatment planning and dose analysis for interstitial photodynamic therapy of prostate cancer," *Phys. Med. Biol.* **54**(8), 2293–2313 (2009).
10. M. S. Patterson, B. C. Wilson, and R. Graff, "*In vivo* tests of the concept of photodynamic threshold dose in normal rat liver photosensitized by aluminum chlorosulphonated phthalocyanine," *Photochem. Photobiol.* **51**(3), 343–349 (1990).